Innovative Food Science and Emerging Technologies 95 (2024) 103726

Contents lists available at ScienceDirect

Innovative Food Science and Emerging Technologies

journal homepage: www.elsevier.com/locate/ifset

# Esterification and volatile compound manipulation using radiofrequency cold plasma

George R. Warne [a,b,e], Mui Lim [a,e], Pradeep Lamichhane [c], Zdenko Machala [d], Volker Hessel [b,c], Philip M. Williams [f], Ian D. Fisk [a,e,*]

[a] International Flavour Research Centre, Division of Food, Nutrition and Dietetics, University of Nottingham, Sutton Bonington Campus, Loughborough LE12 5RD, United Kingdom
[b] School of Chemical Engineering, University of Adelaide, North Terrace Campus, Adelaide, South Australia 5005, Australia
[c] School of Chemical Engineering, University of Warwick, Coventry CV4 7AL, UK
[d] Faculty of Mathematics, Physics and Informatics, Comenius University Bratislava, 84248 Bratislava, Slovakia
[e] International Flavour Research Centre (Adelaide), School of Agriculture, Food and Wine and Waite Research Institute, The University of Adelaide, PMB 1, Glen Osmond, South Australia 5064, Australia
[f] Molecular Therapeutics and Formulation, School of Pharmacy, University of Nottingham, University Park Campus, Nottingham NG7 2RD, UK

ARTICLE INFO

*Keywords:*
Plasma
Esterification
OES
Aroma
Carboxylic acids
Esters

ABSTRACT

Esters are vital in many industries, including food; however, there are still significant opportunities to improve production efficiency, sustainability, and cost. Cold plasma was trialled as a novel tool to induce esterification. Cold plasma increased the esterification of hexanoic acid and methanol in gas and liquid phases. The use of argon significantly improved methanol-based esterification, when compared to air or nitrogen, of hexanoic acid in a mixed solution. This was attributed to interactions with the increased free hydroxyl radicals and hydrogen atoms produced by the argon-based plasma. However, air-based plasma significantly increased esterification when individually treating hexanoic acid in methanol, which indicates the potential use of different plasmas to induce esterification. Further evidence of this could be detected by analysing the intermediary compounds (from the proposed esterification pathway).

## 1. Introduction

Esters are compounds formed by the condensation reaction of an acid (e.g., fatty acid or carboxylic acid) and an alcohol. The formation of these esters plays an essential role in the food (generation of pleasant aromas from unpleasant carboxylic acid counterparts), biofuel (biodiesel production from food waste via alkyl esterification of free fatty acids), and pharmaceutical industries (increased drug solubility in blood and drug-membrane permeation) (Cubas, Machado, Pinto, Moecke, & Dutra, 2016; De Barros, Azevedo, Cabral, & Fonseca, 2012; Janus et al., 2020; Khan et al., 2021). Naturally present carboxylic acid esters play a key role in food as pleasant aromas (typically fruity, jam, floral, etc.), whereas their carboxylic acid counterparts typically produce more sour, acidic, and cheesy aromas (Du, Plotto, Baldwin, & Rouseff, 2011; Prat, Espinoza, Agosin, & Silva, 2014).

The huge role esters play in foods and drinks means ensuring sustainable (low energy consumption and no harsh chemical catalysts) and low cost-to-yield production of esters (Xu, Minhazul, & Li, 2020). Natural ethyl esters of butanoic acid (ethyl butanoate) are typically extracted from plants and then filtered through fractional distillation or supercritical fluids (e.g., $CO_2$) (Xu et al., 2020). The extraction of this is usually enhanced by enzymatic esterification as they have higher yields (48–98%); however, these enzymes, even in their immobilised state, require organic solvents, separation, and constant hydrolysis steps (Khan et al., 2021; Xu et al., 2020; Zare, Golmakani, & Sardarian, 2020). This increases the cost to over ten times the synthetic generation (Akacha & Gargouri, 2015), which is less appealing to consumers and is less environmentally sustainable as it requires inorganic solvents (Khan et al., 2021). Separation costs of the catalyst and additional reactants contribute significantly to the cost hence why novel treatments such as cold plasma or microbubble treatment (ozone microbubbles) may improve this as they don't require catalysts (Abdul-Majeed, Al-Thani, &

* Corresponding author at: International Flavour Research Centre, Division of Food, Nutrition and Dietetics, University of Nottingham, Sutton Bonington Campus, Loughborough LE12 5RD, United Kingdom.
*E-mail address:* Ian.Fisk@nottingham.ac.uk (I.D. Fisk).

https://doi.org/10.1016/j.ifset.2024.103726
Received 28 November 2023; Received in revised form 21 May 2024; Accepted 30 May 2024
Available online 31 May 2024

Al-Sabahi, 2016; Zimmerman & Kokoo, 2018). As numerous other studies have been done on microbubble-induced esterification (reactant microbubbles), cold plasma was trialled (Ahmad et al., 2019; Asif et al., 2024; Istkhar et al., 2023; Javed et al., 2023; Khan et al., 2021). Cold plasma (gas ionised at low temperatures through electrical stimuli (Pan, Cheng, & Sun, 2019)) has previously been shown to enhance methanol and long chain fatty acid esterification (Abdul-Majeed et al., 2016; Cubas et al., 2016), however its role in the esterification of alcohol and short chain carboxylic acids is still unknown (Cubas et al., 2016).

Cold plasma contains many reactive species, including cations (e.g., $H^+$), anions (e.g., $OH^-$), free electrons, UV light, as well as energised atoms and molecules. These can form primary (initial ion formation) and secondary ions (primary ions that interact with the ambient air or liquid solution, which form new ions) that interact with the food (Klämpfl et al., 2012; Misra, Pankaj, Segat, & Ishikawa, 2016; Pan et al., 2019; Warne et al., 2021). RF plasma uses alternating electrodes (outer and inner cylindrical electrodes) to generate an electromagnetic field in the centre with a controlled gas flow in the middle that is ionised by the electrons in the electromagnetic field (Thirumdas, Sarangapani, & Annapure, 2014).

The thermodynamic properties of these ions and electrons in the plasma systems are impacted by energy input and distance from the source (Aanesland, Bredin, Chabert, & Godyak, 2012; Li, Ostrikov, & Sun, 2018). The changes to these properties alter the energy imparted during the mechanistic interactions with the compounds (Pho et al., 2023). By using optical emission spectroscopy (OES) on different gas types for the plasma, the thermodynamic properties could be monitored and correlated to the ionic and excited species output and potential changes to compounds such as carboxylic acid.

Although some studies have found plasma can modify some aromas, the chemical mechanisms and products of this have yet to be fully understood (Campelo et al., 2020a; Campelo et al., 2020b; Liu et al., 2021; Silveira et al., 2019; Warne et al., 2021; Warne et al., 2023). The current study focused on how radiofrequency cold plasma enhances food flavour by esterifying carboxylic acids in ethanol and methanol solutions and how the ions produced by different plasmas could impact esterification reactions. Ethyl and methyl esters of butanoic and hexanoic acids were chosen based on their change in aroma from cheesy and acidic to fruity, nutty, and sweet.

## 2. Materials and methods

### 2.1. Reagents and solvent preparations

Reagents (ethyl butanoate, ethyl hexanoate, methyl butanoate, methyl hexanoate, butanoic acid, hexanoic acid, γ-decalactone, furaneol, and mesifuran) and solvents (ethanol, methanol, and propylene glycol) were all purchased from Sigma Aldrich (Gillingham, UK). Calibration curves were generated for each reagent in ethanol, methanol, or propylene glycol at concentrations from 0 to 0.08% *w*/w. Ethyl butanoate, mesifuran, furaneol, and γ-decalactone were all added as reference aroma compounds to highlight how esterification might work with their typical aroma counterparts present (i.e., in strawberries) (Du et al., 2011; Prat et al., 2014; Warne et al., 2023).

Volatile compounds were prepared in the following ways: 100 μL solutions of ethyl butanoate, butanoic acid, hexanoic acid, furaneol, and γ-decalactone (combined) at 0.01% w/w in methanol (M1) or at 0.01% w/w in propylene glycol (PG1); 100 μL of a 0.05% w/w solution of ethyl butanoate, butanoic acid, hexanoic acid, furaneol, and γ-decalactone in methanol (M2); 300 μL of 0.05% w/w solutions of butanoic acid in ethanol (BaE1), hexanoic acid in ethanol (HaE1), butanoic acid in methanol (BaM1), or hexanoic acid in methanol (HaM1). All these samples were treated on filter paper using the set-up shown in Fig. 1a. Butanoic acid (BaM2) (40 mL at 0.05%*w*/w) in methanol and hexanoic acid (HaM2) (40 mL at 0.05%w/w) in methanol were separately cold plasma treated (C6) (Table 1) within a 30 mm × 30 mm conical vortex (magnetically stirred at 400 RPM) shown in Fig. 1b. Samples were stored in 7 mL clear glass vials (in the dark) with a PTFE lid at 4 °C before and after treatments, as shown in Table 1.

### 2.2. Cold plasma treatments

Samples were cold plasma treated within 36 h of preparation using setups shown in Fig. 1 for treatments shown in Table 1. Analytical measurements were all conducted within a week of treatment with the gas chromatography mass spectrometer (GC–MS), and APCI-MS data was collected within a few hours of treatment.

Two radiofrequency (RF) plasma systems were evaluated: one with a 65 V DC input (2–3 kV AC output at 1 MHz) (kINPen IND, Neoplas GmbH, Greifswald, Germany) and one with a 110 V (50 Hz) DC input (2–3 kV AC output at 1 MHz) (kINPen IND-x, Neoplas GmbH). The output of these devices was approximate and cannot be measured, although it is assumed to be proportional to the input power.

All plasmas were purged for 15 mins prior to each experiment. Unless otherwise stated, all solutions were treated in quintuplicate. Non-treated control samples (C0) were freshly aliquoted for each experiment.

#### 2.2.1. kINPen IND-x

The kINPen IND-x generated 2–3 kV AC output (1 MHz) direct RF-based cold plasma at room temperature (18 to 22 °C), ambient humidity (37.5%), and atmospheric pressure. Plasma temperature and humidity were recorded at 24.9 ± 5 °C and 22.5 ± 1%, respectively (CHY 110 infrared thermometer (Jutech Electric & Electronic Pte Ltd., Singapore) and Rotionic hygrometer A1 (Rotronic Instruments (UK) LTD, Crawley, UK)).

This plasma used the Gas Mixing Unit II-2 (GMU II-2, Neoplas gmbH)

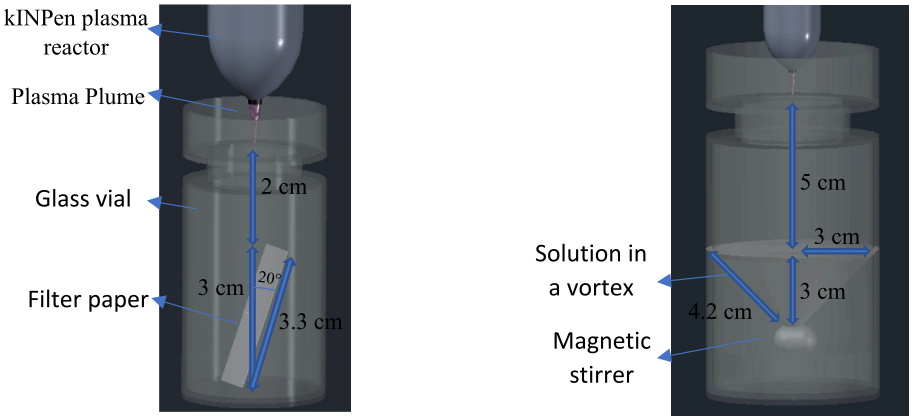


**Fig. 1.** Plasma system setup for direct application onto paper strips (a) or into a vortex (b).

**Table 1**
Experimental conditions of cold plasma treatments with the kINPen IND or IND-x with a 2-3 kV AC output (1 MHz).

| Figure number | Experiment and Sample codes | Cold plasma treatment | Plasma source | Container - delivery | Exposure time (seconds) and plasma to source distance (cm) | Gas used and flow rate |
|---|---|---|---|---|---|---|
| NA | All | C0 | N/A | Varied | 0 s; N/A | N/A |
| Fig. 2 | 100 µL of M1<br>100 µL of PG1 | C1 | kINPen IND-x | Polypropylene – aroma paper strips[1] | 0 s; N/A | 4 L·min$^{-1}$ Air |
| | 100 µL of M1 | C2 | | | 60 s; 2–5 cm | 4 L·min$^{-1}$ Air |
| Fig. 3 | 100 µL of M2 | C3 | kINPen IND-x | Glass – aroma paper strips[1] | 60 s; 2–5 cm | 4 L·min$^{-1}$ Air<br>4 L·min$^{-1}$ Ar<br>4 L·min$^{-1}$ $N_2$ |
| | | C4 | | | | |
| | | C5 | | | | |
| Fig. 4 | 300 µL of BaM1 or HaM1 | C3 | kINPen IND-x | Glass-aroma paper strips[1] | 60 s; 2–5 cm | 4 L·min-1 Air |
| Fig. 5 | 300 µL of BaE1 and HaE1 | C3 | kINPen IND | Glass-aroma paper strips[1] | 60 s; 2–5 cm | 4 L·min-1 Air |
| Fig. 6 | 40 mL of BaM2 or 40 mL of HaM2 | C6 | kINPen IND | Glass – liquid in 30 × 30 mm Φ vortex[2] | 300 s; 5–8 cm | 4 L·min$^{-1}$ Air |
| Fig. 7 | 300 µL of BaE1, HaE1, BaM1, and HaM1[3] | C3 | kINPen IND | Glass-aroma paper strips[1] | 60 s; 2–5 cm | 4 L·min-1 Air |

[1] Premium aroma assessment papers, purchased from LS Materials, Sudbury, UK. Setup shown in Fig. 1a.
[2] Setup shown in Fig. 1b.
[3] Setup shown in Supplementary Fig. 1

with its respective software (kINPen_GMUII, Neoplas GmbH) to control the gas flow (more accurate as it accounts for gas densities) into the kINPen IND-x.

#### 2.2.2. kINPen IND

A kINPen IND (Neoplas) plasma reactor was used without a GMU-II unit, as described by Pho et al. (2023). The kINPen IND was also operated at 2–3 kV AC (1 MHz) output. However, the input could not be controlled and was fixed at 110 V. 4 L·min$^{-1}$ argon was used for argon-based plasma and 4 L·min$^{-1}$ of air for air-based plasma. The flow rate setting is based on argon density; hence, a displayed value of 4.3 L·min$^{-1}$ (what air was set to) is approximately 4 L·min$^{-1}$ for air. Ambient temperature and humidity were 22.3 °C and 44.9%, respectively; Plasma temperature and humidity were 22.1 °C and 39.0%, respectively (Protmex PT 6508, Protech International Group Co., Ltd., Shenzhen, China).

### 2.3. Gas chromatography-mass spectrometry (GCMS)

Headspace solid-phase microextraction (HS-SPME) was carried out using a 50/30 µm DVB/CAR/PDMS 1 cm fibre (Supelco, Sigma Aldrich, UK) and used for all headspace SPME analysis. Samples treated with C0, C1, C2, C3, C4, & C5 were extracted into the gas chromatograph (GC) (Trace 1300 Gas chromatograph, Thermo Fisher Scientific Inc., Waltham, USA) mass spectrometer (MS) (ISQ QD single quadrupole Mass Spectrometer, Thermo Fisher Scientific Inc., Waltham, USA) (GCMS) (method adapted from Lester et al., 2021). These samples were heated at 37.5 °C for 10 min, extracted for 20 min, and desorbed for 3 mins into the ZB-Wax column (30 m × 0.25 mm I.D.). This column was kept at 40 °C for 2 mins and increased to 240 °C at a rate of 6 °C·min$^{-1}$, then maintained at 240 °C for 5 min. Helium was used with a splitless flow of 18 psi. Full MS spectra were acquired (35–300 *m/z*). The data was then background subtracted, deconvoluted, and integrated using TraceFinder 5.1 with the Deconvolution Plugin 1.2 (Thermo Fisher Scientific Inc., Waltham, USA), and compounds were identified through NIST 17 (National Institute of Standards and Technology, Gaithersburg, USA) and their respective calibration curves.

The HS-SPME extraction (50/30 µm DVB/CAR/PDMS 1 cm fibre) of samples treated with C6 and C0 was conducted using the GC (Agilent 8860) MS (Agilent 5977B GC/MSD) with a Wax column (30 m × 0.25 I.D. DB Wax) (Agilent, Santa Clara, USA). These samples were heated at 37.5 °C for 10 min extracted for 20 min, before 3 mins of desorption into the wax column.

Partition coefficients of methanol/air (for solutions with a methanol base) and ethanol/air (for solutions with an ethanol base) were calculated (Eq. (1)) for hexanoic acid, methyl hexanoate, ethyl hexanoate, butanoic acid, methyl butanoate, and ethyl butanoate (Supplementary Table 1) (Li et al., 2023). These were used to determine the true headspace concentration of the reference standards (Eq. (2)). Which were then used to calculate the true headspace concentration of the samples with isolated compounds (C0, C3, & C6; Figs. 4 & 5), using calibration curves.

$$K_{ax} = \frac{K_{aw}}{e^{\left(\frac{\Delta G}{R \times T}\right)}} \quad (1)$$

where, '$K_{ax}$' is either the methanol/air partition coefficient ($K_{am}$) or the ethanol/air partition coefficient ($K_{ae}$), '$K_{aw}$' is the water/air partition coefficient, '$\Delta G$' is the change in solvation free energy between the solvents taken as 22.175 KJ/mol for methanol (Zhong, Warren, & Patel, 2008) and 21.14 KJ/mol for ethanol (Ben-Naim & Marcus, 1984), 'R' is the gas constant (8.314), and 'T' is the temperature (294.15 Kelvin) (Li et al., 2023). $K_{aw}$ values were taken from EPIWEB v4.1 (EPI Suite, Environmental Protection Agency, Washington, DC, USA).

$$C_h = C_{lq} \times K_{ax} \quad (2)$$

where, and '$C_h$' is the headspace concentration of the compound, & '$C_{lq}$' is the liquid concentration.

Liquid extraction of C6 and C0 was conducted using a similar method to Favell et al. (2022). 3 mL of each sample were extracted, mixed with 2 mL of a 6:1 hexane-ethyl acetate solution, and then centrifuged (3000 rpm for 10 mins). Approximately 1.5 mL of the top organic layer was extracted for GCMS analysis. The liquid concentration calibration curves (0–0.125% *w*/w) were calculated for methyl butanoate, methyl hexanoate, butanoic acid, and hexanoic acid (all had 20 µL of 102.5 mg·L$^{-1}$ d6-syringol (in 9:1 water-ethanol)). 50 µL of the extracted sample was injected into a GC (Agilent 6890 N) MS (Agilent 5973 N MS) with a wax column (60 m × 0.25 I.D. DB Wax) (Agilent, Santa Clara, USA). For both liquid and headspace extraction of samples treated with C0 and C6, the DB-wax columns were kept at 40 °C for 2 mins and increased to 240 °C at a rate of 6 °C·min$^{-1}$ then maintained at 240 °C for 5 min. Helium was used with a splitless flow of 27 psi. Full MS spectra were acquired for 30–350 *m/z*. The data for samples treated with C0 and C6 were processed using Agilent Unknowns Analysis software 7.0.457.0 (Agilent Inc., Santa Clara, USA), and compounds were identified through NIST 20 (NIST) and their respective calibration curves.

### 2.4. Real-time volatile analysis

Samples BaE1, HaE1, BaM1, & HaM1 treated with C0 & C3 were analysed in real-time on the atmospheric pressure chemical ionisation mass spectrometer (APCI-MS) (APCI Quattro Ultima, Micromass, Wythenshawe, UK) in single ion recording mode for each compound using methods adapted from Lester et al. (2021). This APCI-MS was attached to an MS-nose (Micromass) (a heated fused silica tubing (1 m × 0.53 mm i.d.; 160 °C)) with the set-up shown in Supplementary Fig. 1. Briefly, the following settings on Mass lynx 4.1 (Waters Corporation, Milford, USA) were used: ES+ ionisation source, cone voltage 30 V, capillary voltage 8 eV, source temperature 60 °C, and desolvation temperature 20 °C.

### 2.5. Optical emission spectroscopy

The ionic and excited species output of the argon- and air-based plasma were determined through optical emission spectroscopy (OES) using the methods of Bao, Reddivari, and Huang (2020). This used an HR2000+ spectrophotometer with a 200 nm to 1000 nm collimating lens (Ocean Optics Inc., Dunedin, Florida, USA). For the 2D analysis, measurements were taken 5 mm from the end of the plasma plume (axially) when analysing the air or argon plasma (0 and 12 mm away from the plasma exit, respectively). The fibre was directed at the plasma at a straight angle (180°) inside a dark cylindrical ABS polymer container (Supplementary Fig. 2) (10 replicates were taken from one point). For cross-sectional OES examination of Argon-based plasma (this was not possible with air due to the small size of the air-plasma), the fibre was placed through 1.5 mm holes (2 mm apart centre to centre) of a 20 × 20 cross-sectional grid inside a black ABS container and recorded in quintuplicate (Supplementary Fig. 3). Data was recorded using Oceanview 2.0.8 software (Ocean Optics Inc., Dunedin, Florida, USA). Matplotlib (3.7.1) was used in conjunction with Python (3.11.2), Pandas (2.0.1), Seaborn (0.12.2), and Numpy (1.24.3) (Python Software Foundation, Delaware, USA), to generate the 3D plots of the OES cross-sectional data.

### 2.6. Electron and gas temperatures

The plasma's rotational and transitional gas temperatures were estimated using the Boltzmann plot, and the electron temperature was calculated through collisional radiative modelling as described by Ghimire et al. (2017).

### 2.7. Statistical analysis

The statistical significance ($P < 0.05$) of mass spectrometry data was determined using ANOVA and either Games Howell or Tukey post hoc tests using SPSS (SPSS v27.0.1.0 64-bit edition for Windows, IMB Corporation, New York, USA) (based on homogeneity of variance tests: $P > 0.01$ meant Tukey test was used). Microsoft Excel 365 (Microsoft Corporation, Redmond, USA) was used for data processing. Unless otherwise stated, all samples were treated in quintuplicate, and a double Grubbs test was used to identify outliers ($P < 0.001$) (XLSTAT 2021.1.1, Addinsoft, New York, USA). Detected outliers were removed if they increased CV by >20%.

## 3. Results and discussion

The esterification of butanoic acid and hexanoic acid was evaluated under different sample (matrix, competing compounds, and base solvents) and plasma (gas type) conditions and then compared against OES data to determine mechanistic interactions.

### 3.1. Impact of solvents on butanoic and hexanoic acid esterification

Cold plasma significantly increased four aroma compounds (including butanoic acid (2.85× increase) and hexanoic acid (3.51× increase)) when in methanol-based solvents. However, this air-based plasma did not significantly impact butanoic and hexanoic acid in propylene glycol (control solvent) (Fig. 2). Although plasma-treating methanol might lead to a decrease in the concentration of these compounds, through evaporation extraction, the evaporation would have occurred in a similar extent with gas as well as plasma treatments. The increase is therefore likely due to other influences such as methanol and plasma interactions(Fig. 2).

It could be suggested that the increase is caused by the cold plasma evaporating the methanol and potentially altering the concentration. However, if this was the case, ethyl butanoate and γ-decalactone should also have increased (Fig. 2). Since there is little additional thermal energy in the plasma (297 K) (compared to the surrounding air (293 K)), most of the additional evaporation that occurs should be through the kinetic energy of the gas itself (Nagata, Usui, & Bonn, 2015). Hence, if the changes were primarily caused by evaporation, then there should be significant differences between the solvent matrices when treated with just the gas for all samples. However, for butanoic acid and hexanoic acid, there was a significant increase when in methanol (Fig. 2).

### 3.2. Effects of gas type on the esterification efficacy of plasma

When treating a mix of volatile compounds, ethyl butanoate significantly increased when treated with air-based cold plasma, but this was not seen when treated with nitrogen or argon (Fig. 3). This suggests that the reactive oxygen species (e.g., OH, $OH^-$, O, $O^+$) produced by the air-based plasma in the primary interaction stage are impacting the chemistry of ethyl butanoate (Klämpfl et al., 2012). It is worth noting, however, that the volatility of the methyl and ethyl esters are considerably higher than their carboxylic acid counter parts and as such plasma may just be enhancing the volatility to test this liquid based analysis was performed (Supplementary Table 1; Section 3.4). Mesifuran, however, only significantly increased when treated with Argon, the most inert of the gases tested. Both butanoic acid and hexanoic acid were affected significantly by the $N_2$ and air-based cold plasma treatments. Since there were no significant changes between the $N_2$ and air-based CP treatments of these acids, it is likely that the reactive nitrogen species (e.g., $N_2$, $N_2^+$), and perhaps their secondary interaction stage derivatives, form the principal mechanistic factors in the alteration of the butanoic acid and hexanoic acid chemical structure (Fig. 3). Despite this, γ-decalactone appeared relatively stable and was not significantly affected by any of these three different cold plasma treatments. Interestingly, the methyl ester of hexanoate was only increased under argon-based cold plasma. By comparing the OES spectra of argon and air-based plasmas it may be possible to determine which unique ions, excited atoms, or excited molecules could be causing this large increase in methyl hexanoate in the headspace.

### 3.3. Esterification impact of direct application on individual compounds

Analytes were also treated individually to ensure they were not competing with or obscuring the products of the other compounds. Interestingly, the cold plasma significantly increased the apparent esterification of methanol and hexanoic acid to give methyl hexanoate (Fig. 4). This was contradictory to what was observed when treating all compounds in the same solution (Fig. 4), which could suggest other compounds interfere with the potential esterification process. Methyl butanoate also appeared to increase, although this was not statistically significant (Fig. 4).

Headspace butanoic acid and hexanoic acid significantly increased after cold plasma treatment (Fig. 5). This agrees with results obtained from methanol, which could suggest similar chemical changes are

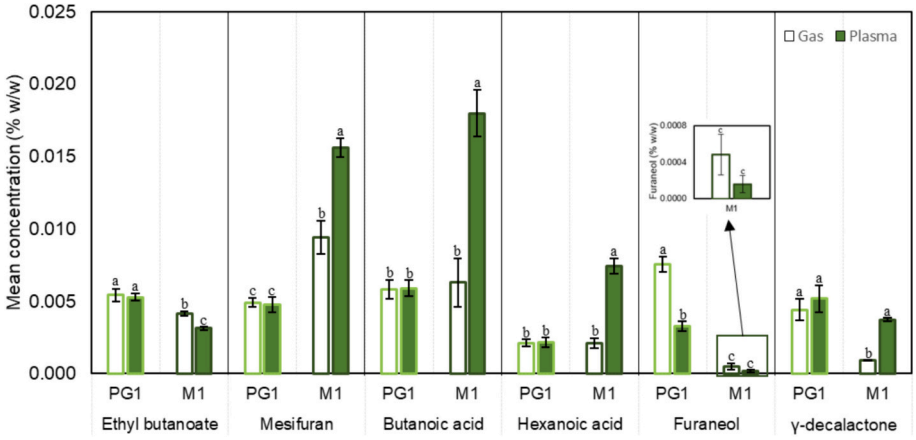


**Fig. 2.** Mean estimated headspace concentrations based on headspace volatile analysis ($n = 3$–5) (±s.d) of ethyl Butanoate, mesifuran, butanoic acid, hexanoic acid, furaneol, and γ-decalactone in a mix of these volatiles in propylene glycol (PG1) or methanol (M1) using 4 L·min$^{-1}$ air-based direct RF plasma (plasma) (C2) or non-ionised air (also at 4 L·min$^{-1}$) (gas) (C1) (kINPen IND-x;2–3 kV AC (1 MHz) output), for 60 s. Letters indicate significant differences ($P < 0.05$). Methyl butanoate and methyl hexanoate were below the limit of detection in these samples.

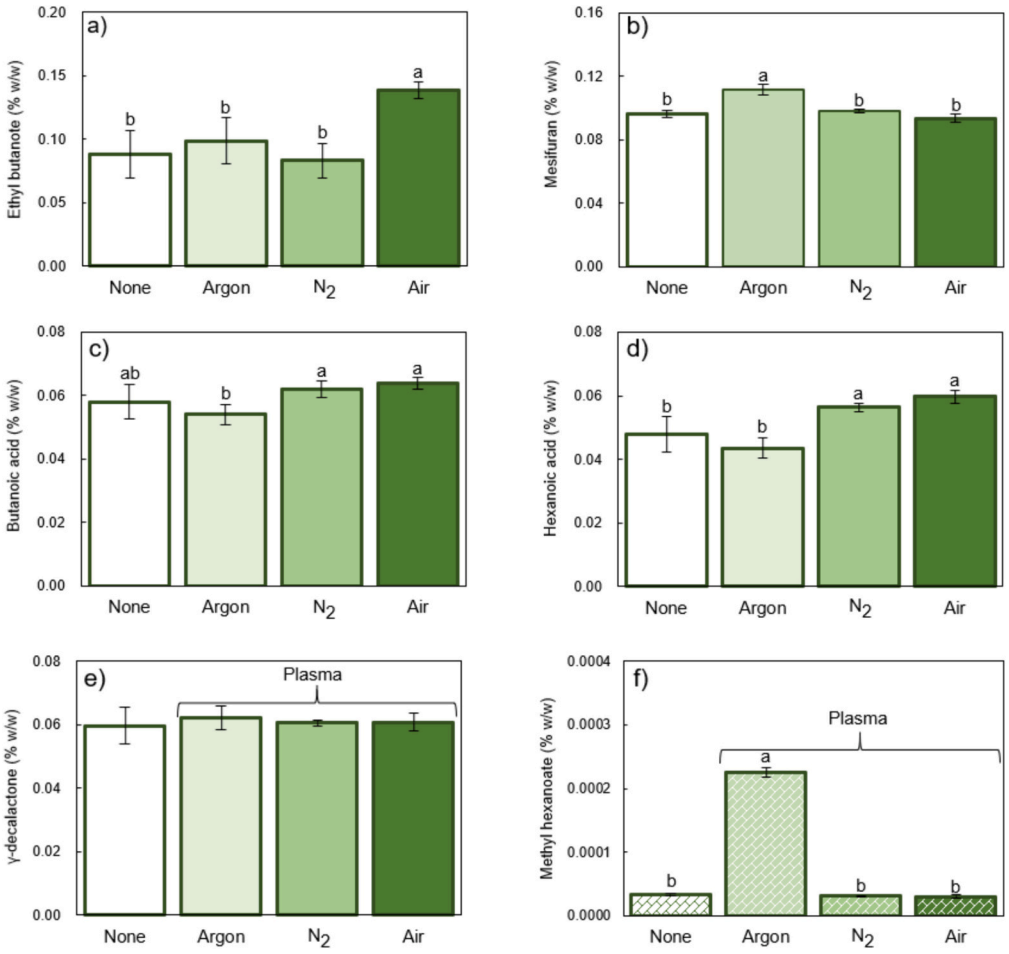


**Fig. 3.** Mean estimated headspace concentrations (n = 3–5) (% *w*/w) based on headspace volatile analysis (±s.d) of ethyl butanoate (**a**), mesifuran (**b**), butanoic acid (**c**), hexanoic acid (**d**), γ-decalactone ($P > 0.05$) (**e**) and methyl hexanoate (**f**) from a mix of these compounds in methanol (M2) after no treatment (C0), argon-based plasma treatment (C4), nitrogen-based plasma treatment (C5), or air-based plasma treatment (C3) at 4 L·min$^{-1}$ for 60 s at 2–3 kV AC (1 MHz) output). Different letters indicate significant differences ($P < 0.05$).

occurring (Fig. 2). However, unlike those in methanol, potential esterification was not observed in ethanol in either the non-CP-treated control or CP-treated samples (i.e., ethyl butanoate and ethyl hexanoate were not observed in the samples).

### *3.4. Liquid phase analysis of butanoic and hexanoic acid after plasma treatment*

Liquid phase butanoic and hexanoic acid concentrations appeared to

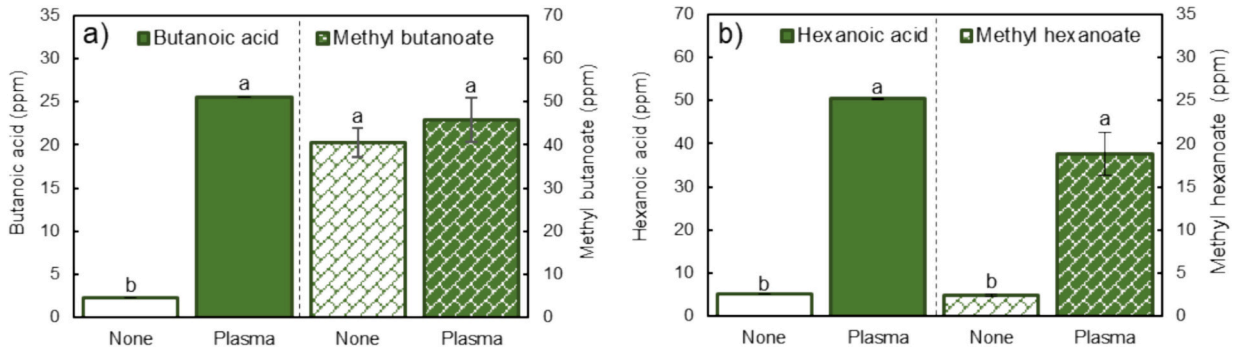


**Fig. 4.** Mean (± s.d.; $n = 8–10$) calculated headspace volatile concentrations of butanoic acid and methyl butanoate (a), and hexanoic acid and methyl hexanoate (b) in methanol solutions of butanoic acid (BaM1) and hexanoic acid (HaM1), respectively. These were treated with (C3) or without (C0) 4 L·min$^{-1}$ air-based plasma (kINPen IND-x) for 60 s (2–3 kV AC output at 1 MHz). Different letters within each compound indicate significant differences ($P < 0.05$).

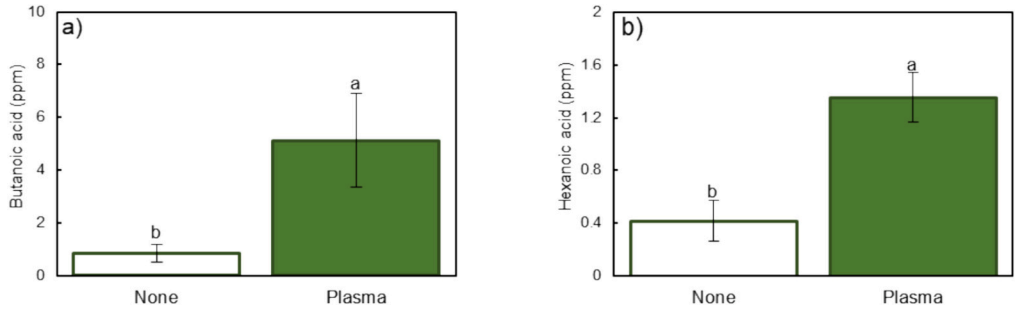


**Fig. 5.** Mean calculated headspace volatile concentrations ($n = 3–4$) (±s.d.) of butanoic acid (a) and hexanoic acid (b) from butanoic acid (BaE1) or hexanoic acid (HaE1) in ethanol (respectively), with (plasma) (C3) and without (none) (C0) air-based plasma treatment (4 L·min$^{-1}$) with the kINPen IND for 60 s. Ethyl butanoate and ethyl hexanoate were below the limit of detection. Different letters indicate significant differences ($P < 0.05$).

increase (Fig. 6) (as well as in the gaseous phase (Fig. 4)). Cold plasma also significantly increased the abundance of methyl hexanoate within the solution of hexanoic acid in methanol (Fig. 6b). This suggests an esterification yield of 0.0159 ± 0.0036% without any treatment compared to 0.1198 ± 0.0368% with cold plasma treatment (a 7.5 × increase). This agrees with the increased presence of methyl hexanoate observed in the headspace (Fig. 4) and strongly suggests that these cold plasma treatments can induce esterification and not just increase the volatility of the methyl esters. Argon plasma was able to esterify hexanoic acid, whereas air-based plasma could only esterify when treating hexanoic acid individually.

Abdul-Majeed et al. (2016) found that plasma treatment increased esterification of long chain fatty acids and methanol. The current study was able to increase esterification short chain fatty acids even at relatively short treatment times (5 mins for a 0.12% yield) (Fig. 6). The treatment times in the study by Abdul-Majeed et al. (2016) was considerably longer and increased yield was found to be directly correlated with increased treatment time (33% at 40 mins to 72% at 100 mins). While these treatment times can be trialled for esterification of short chain fatty acids, direct application on food for this long may lead to detrimental quality changes (Warne et al., 2021).

It is also worth mentioning that the increase in input power in the kINPen IND (compared to the kINPen IND-x) could have increased the energy levels of the electrons and ions produced, thereby increasing the OH radical generation, which may have impacted the OES data obtained from the kINPen IND (Pandiyaraj et al., 2020; Reuter, Von Woedtke, & Weltmann, 2018)

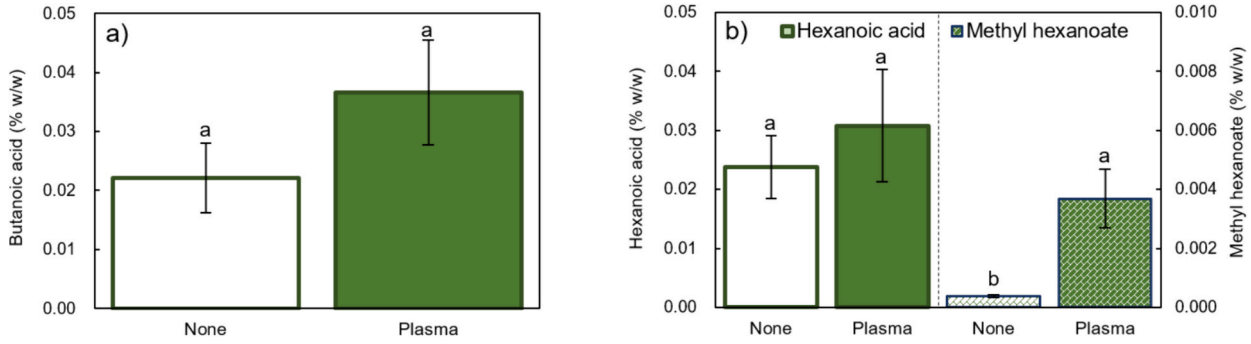


**Fig. 6.** Mean (± s.d.) ($n = 5$) liquid volatile concentrations (% *w*/w) of butanoic acid in a solution of butanoic acid in methanol (BaM2) (a) and the liquid concentration (% w/w) of hexanoic acid and methyl hexanoate in a solution of hexanoic acid in methanol (HaM2) (b) with (C6) or without (C0) 300 s of 4 L·min$^{-1}$ air-based cold plasma treatment 2–3 kV AC (1 MHz) output (kINPen IND). Different letters within each compound indicate significant differences ($P < 0.05$).

### 3.5. Real-time analysis of ester formation using cold plasma and an MS-nose-APCI-MSMS

Air-based plasma treatment (C3) of butanoic acid in methanol induced significantly increased butanoic acid and methyl butanoate headspace volatiles during the first 60 s after treatment (initial headspace) (Fig. 7). This plasma-induced increase in methyl butanoate was not observed in analyses conducted in the subsequent days (post-treatment) (Figs. 3, 4, & 6), which indicated a shorter volatility of this ester. Methyl hexanoate was also significantly increased when plasma treating hexanoic acid in methanol, which substantiates the data from the previous analysis (Figs. 3, 4, & 6), which indicated that plasma treatment significantly increased the methyl esterification of hexanoic acid. Butanoic acid (31%; not significant ($P > 0.05$)) and hexanoic acid (>55%; significantly higher than the noise ($P < 0.05$)) increased in the initial headspace (Fig. 7) when plasma treated in ethanol, similar to the increase observed in the post-treatment analysis (Fig. 5).

### 3.6. Optical emission spectroscopy (OES) analysis

OES analysis was used to determine what ions and excited species are produced by air and argon-based RF plasmas. This would help explain potential ions and excited species that are key to the esterification reaction.

#### 3.6.1. Two-dimensional OES analysis of air-based and argon-based plasma

Air-based plasma contains (based on semi-quantitative OES), in order of signal intensity, $N_2$ ($C^3\Pi_u \rightarrow B^3\Pi_g$), OH ($A^2\Sigma^+ \rightarrow X^2\Pi$), $N_2^+$, $H_\alpha$, O (4S(3P)➔4S(3S)) (Fig. 8a & 8b). Argon plasma contained substantially more O, $H_\gamma$, and OH ions than air plasma (Fig. 8c), which could explain why argon increased the esterification even when other compounds were present and competing (Fig. 3e). This was similar to Bao et al. (2020), who found that argon and helium plasmas have higher reactive oxygen (OH) and nitrogen ($N_2^+$) ions, which was attributed to penning ionisation. This meant potential increased secondary interactions of metastable atoms and molecules with other molecules in the air (e.g., water) (highly energised argon and helium atoms with longer half-lives), which ionised the O, H and N atoms (as they have lower ionisation potentials). Bao et al. (2020) also found that nitrogen and air-based DBD plasma had similar compounds ($N_2$, $N_2^+$, and OH), with $N_2$ being more prevalent in nitrogen-based cold plasma; However, they did not find neutral oxygen in either air or nitrogen. The air-based RF plasma in the current study, also appeared to generate neutral oxygen atoms and the spectrum of $N_2$, $N_2^+$, and OH was proportionally similar to the study by Bao et al. (2020), with the exception of NO, $O^+$, and $H_\gamma$ (Fig. 8a & 8b).

#### 3.6.2. 3D cross-sectional OES analysis of argon-based plasma

To understand how these compounds are distributed in the 3D space, a 20 × 20 grid of holes was devised to house the optical fibre at different tangential and axial positions along a cross-sectional plane 2.5 mm away (radially) from the plasma source. The presence of all ions recorded by the OES deteriorated substantially after 7.5 mm away axially and 3.75 mm away tangentially from the plasma source; in fact, only atomic oxygen was still clearly visible 6.25 mm tangentially away from the plasma source (Fig. 9).

### 3.7. Gas and electron temperatures

The gas temperature of the argon-based plasma was calculated to be 107.75 °C (380.9 K), which refers to the average translational kinetic energy (Fig. 10a). The rotational temperature of the $N_2$ molecules was observed to be similar at 380.75 K (Fig. 10a). This similarity indicated

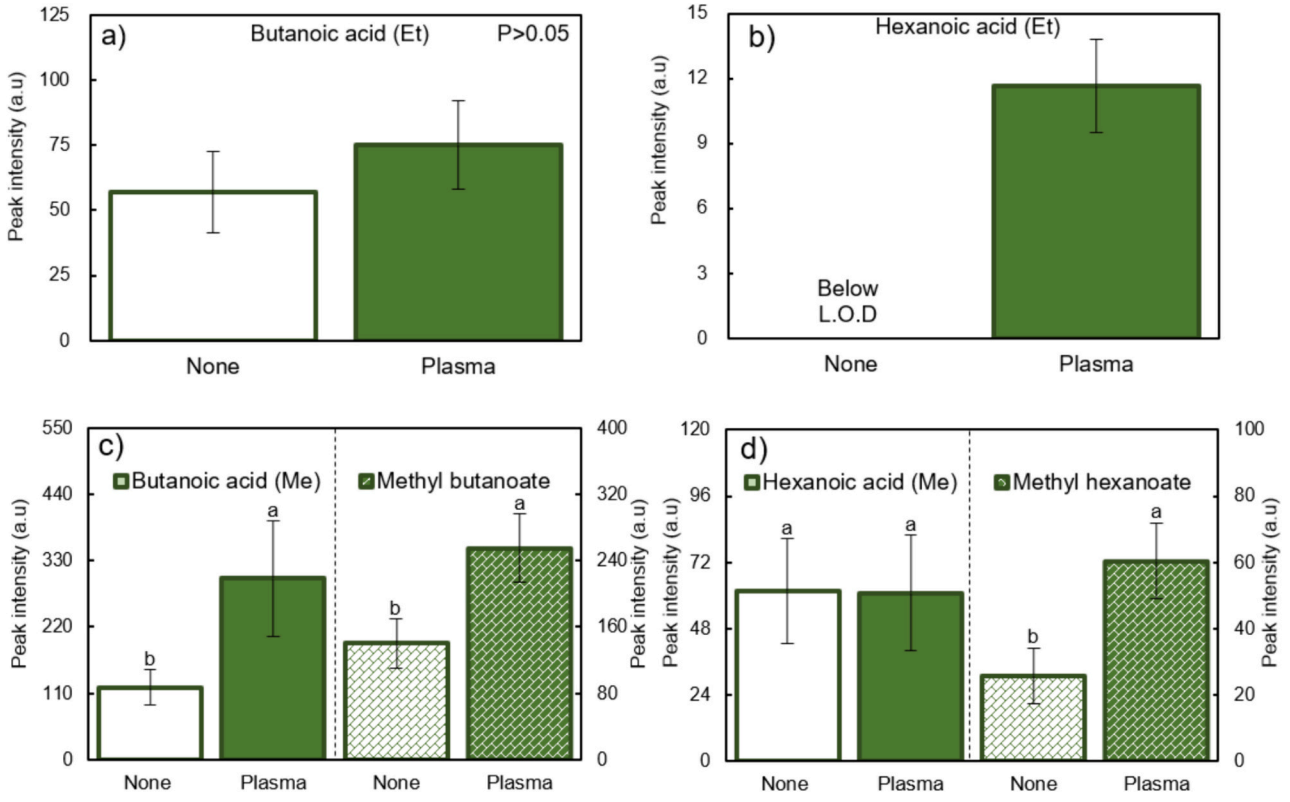


**Fig. 7.** Mean relative intensity (taken from MS-nose APCI-MS analysis) ($n$ = 7 to 9) (± S·D) of butanoic acid (a) in a butanoic acid and ethanol solution (BaE1), hexanoic acid (b) in a hexanoic acid and ethanol solution (HaE1), butanoic acid and methyl Butanoate (c) in a butanoic acid and methanol solution (BaM1), and hexanoic acid and methyl hexanoate (d) in a hexanoic acid and methanol solution (HaM1). These were treated with (C3) and without (C0) 60 s of air-based plasma treatment (kINPen-IND-x). Different letters show significant differences ($P < 0.05$) (set up shown in Supplementary Fig. 1).

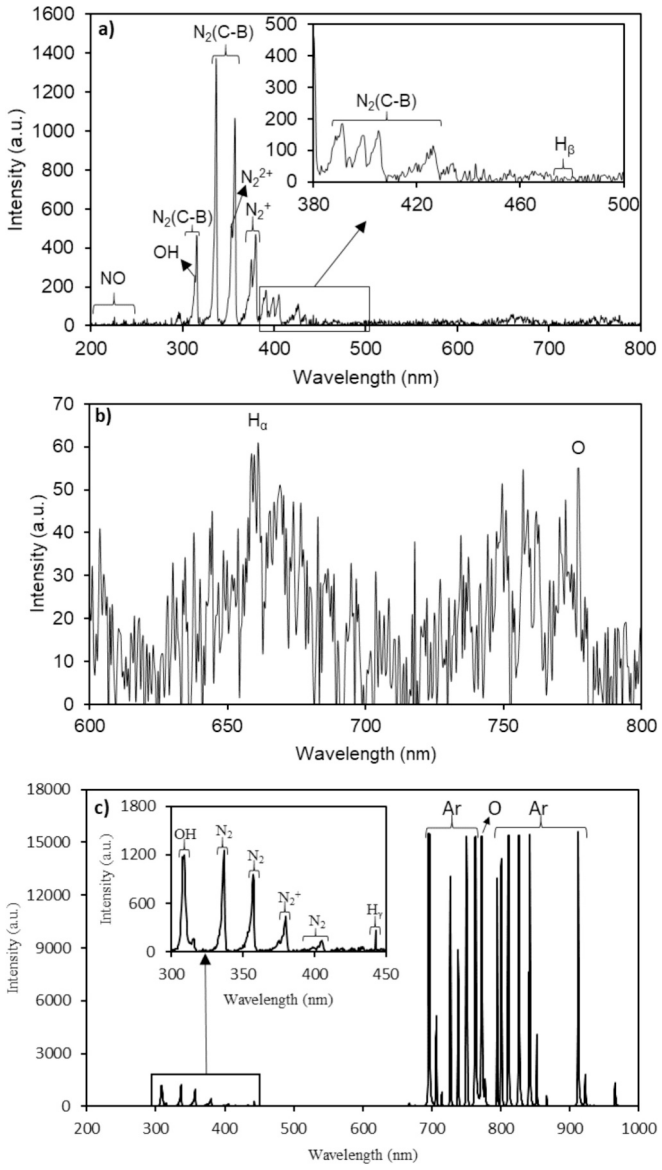


**Fig. 8.** Optical emission spectroscopy (OES) analysis of Air-based RF cold plasma (kINPen IND) at 4 L·min$^{-1}$ and 2–3 kV AC output (a & b) and of Argon-based cold plasma under the same conditions (c) 200 nm to 1000 nm optical fibre was used and aimed directly inside the plasma source and protected from light by a bespoke black cylindrical container (fibre was positioned 12 mm away axially from the exit (~2 mm away from plasma source) for the argon plasma) (Supplementary Fig. 2). Ions and excited atoms and molecules were identified by their commonly associated OES wavelengths (Bao et al., 2020; Golda, Biskup, Layes, Winzer, & Benedikt, 2020; Lotfy, 2020; Machala et al., 2007; Pandiyaraj et al., 2020; Pho et al., 2023; and Tomeková, Kyzek, Medvecká, Gálová, & Zahoranová, 2020).

that the rotational relaxation of the argon gas was very short in the plasma, which typically facilitates consistent excited species interactions through the near thermodynamic equilibrium of the translational and rotational energies of atoms and molecules (Li et al., 2018). Pho et al. (2023) also used the same plasma reactor with argon (although at a reduced flow rate (2 L·min$^{-1}$)) and found that the plasma gas temperature was calculated to have peaked at 348 K and reached a peak thermal conductivity of 0.02 W·mK$^{-1}$ and heat capacity of 0.52 kJ·kg$^{-1}$·K$^{-1}$ suggesting a near uniform spatiotemporal thermodynamic profile (i.e., minimal change in heat capacity with increased gas temperature). They also found that increased gas temperature (298–348 K) increased thermal conductivity; This, therefore, also proportionally increased the diffusivity of the ions, which is linked to increased ionic reaction rates (Pho et al., 2023). However, the gas temperature of the current study was far higher (380.9 K), which suggests the increased flow rate may have increased the thermal conductivity and thermal diffusivity and potentially also ionic reaction rates (Fig. 10a) (Li et al., 2018; Pho et al., 2023). This could explain why argon-based plasma increased the formation of methyl hexanoate even in the multi-compound system (Fig. 3e) and would agree with the findings from OES (Figs. 7c & 8).

The electron temperature was measured as 1.003554 eV (Fig. 10b). This electron temperature affects the electron energy distribution function (increased temperature increases volatility and hence distribution) and the ionisation equilibrium (recombination of electrons with ions will reduce with increased electron temperatures), both of which impact the overall electron-ion coupling (Li et al., 2018). The electron temperature increased with a reduced relative density of argon (Fig. 10b). Using a larger and more powerful (200 W) RF plasma, Aanesland et al. (2012) found low-pressure argon plasma to have electron temperatures far higher (4 eV) than those in the current study, indicating a positive correlation with power output; however, the low pressure would also have impacted this. They also found this to have slightly reduced (~3.2 eV) with increased distance from the plasma source (Aanesland et al., 2012). Although this was relatively small between the 2 cm to 5 cm used in the current study, it is worth noting that the compounds present further away from the plasma may well have reduced electron-ion coupling due to the reduced electron temperatures (Fig. 9b) (Li et al., 2018). Hence, for static samples, the efficacy of the plasma was likely reduced with increased distance from the plasma source. It also means higher energy systems may well increase the formation of the methyl esters of butanoic and hexanoic acid, so higher energy plasma systems could also esterify ethyl esters of these carboxylic acids as well.

### 3.8. Proposed ionic interaction mechanisms

Abdul-Majeed et al. (2016) found that a dielectric barrier discharge (DBD) plasma was able to esterify long-chain fatty acids in methanol in both free and glyceride forms. They attributed this to the initial deprotonation of methanol from the excited electrons and the subsequent reaction with the positively charged C═O group on the fatty acid. Although esterification occurs naturally they also found that plasma lowered the activation energy of this reaction and reduced coproduct (Abdul-Majeed et al., 2016).

With a reduced activation energy, the increase in O, Hγ, and OH reactive species in an argon plasma was likely increasing the esterification reaction at the positively charged C═O group (Fig. 11) (Abdul-Majeed et al., 2016). Hence, would explain the increased abundance of methyl hexanoate in the headspace compared to the other plasmas used (Fig. 3e).

Hence, the potential for reversible esterification reactions between methanol and butanoic acid and methanol and hexanoic acid to form methyl butanoate and methyl hexanoate, respectively, were considered. Cold plasma increased the presence of methyl hexanoate in both the headspace and liquid. The fact that butanoic acid and hexanoic acid did not significantly change when in propylene glycol (i.e., the control solvent) is strong evidence of interaction with methanol. This changes the negatively associated aromas of hexanoic acid (cheesy) to the more positive: methyl hexanoate (fruity/pineapple-like) (Du et al., 2011). Furthermore, in methanol, there is apparent natural and induced (CP treatment) esterification. Despite this, esterification (natural or induced) did not appear to occur in ethanol-based solvents. The implications of this include a new and potentially cheaper method for generating esters compared to the current sulfuric acid-based catalysts (Sarma, Kumar, Vijay, & Ramesh, 2021). It could also allow people to generate more complex esters of carboxylic acids and alcohols (Fischer-Spier esterification) that are not normally viable (Harris, Zhang, & Phan, 2020).

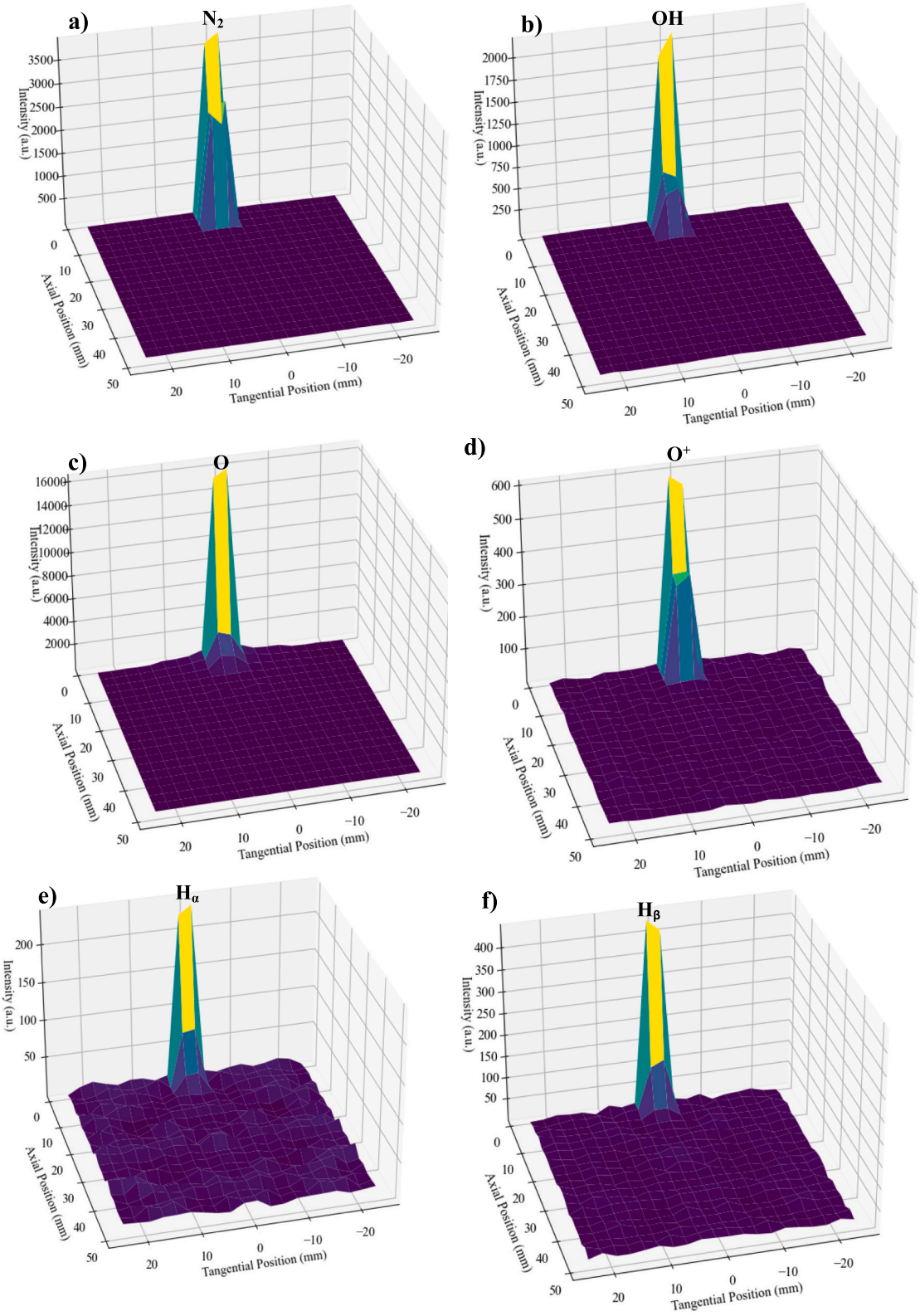


**Fig. 9.** Cross-sectional optical emission spectroscopy (OES) analysis of $N_2$ (330–340 nm) (**a**), OH (300–320 nm) (**b**), $O_1$ (770–780 nm) (**c**), $O_1^+$ (400–410 nm) (**d**), $H_\alpha$ (650–660 nm) (**e**), and $H_\beta$ (480–490 nm) (**f**) in argon-based RF cold plasma (kINPen IND) at 4 L·min$^{-1}$ Argon and 2–3 kV AC output. 200 nm to 1000 nm optical fibre was used and fitted inside holes along the tangential and axial positions of a 20 × 20 grid, 2.5 mm away (radial distance) from the plasma source. This was fitted in a bespoke black box container (ABS plastic) with the inbuilt grid (Supplementary Fig. 3) that isolated the plasma from outside light. Ions were identified from the highest intensity values between the wavelengths stated above for semi-quantitative OES analysis of their associated wavelengths based on values obtained from Bao et al. (2020), Golda et al. (2020), Lofty (2020), Pandiyaraj et al. (2020), Pho et al. (2023), Roy, Talukder, and Chowdhury (2017), Tomeková et al. (2020).

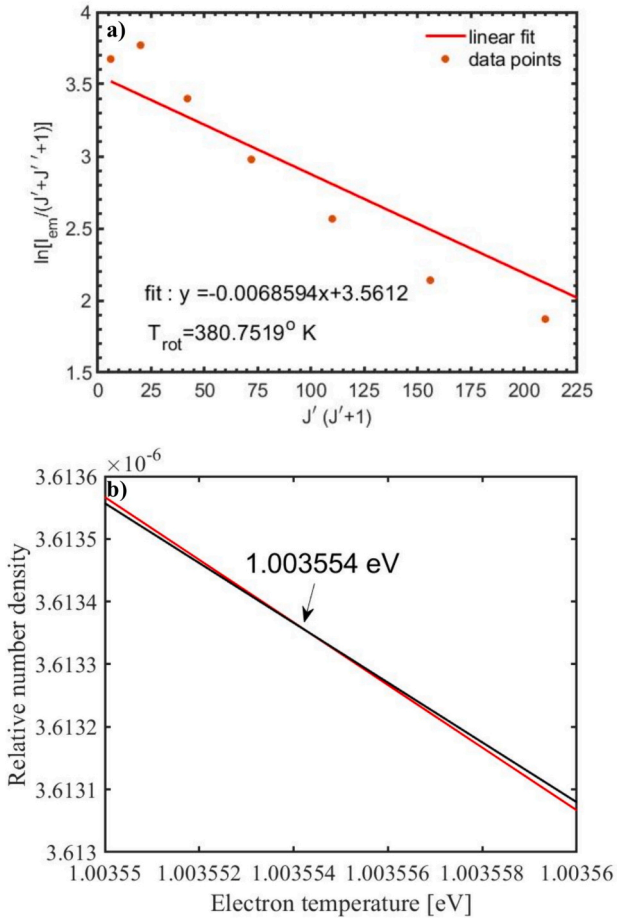


**Fig. 10.** Mean ($n = 5$) gas (**a**) ($R^2 = \sim 0.97$) and electron (**b**) temperatures of the argon-based direct RF plasma (kINPen IND) operating at 4 L·min$^{-1}$. Measured from the argon emission lines using the calculation methods from Ghimire et al. (2017).

Although many ions are produced by these plasmas, it is proposed that OH, H, and free electrons are the key contributors to increasing the presence of esters (Fig. 11). The protonic activation of the carbonyl group of the carboxylic acid is proposed to occur naturally either through hydronium ions present at the air-solution interface or with free H+ ions from the dissociative excitation of the water vapour (also increasing the OH groups from water) (Duignan, Parsons, & Ninham, 2015; Hernández-Montelongo et al., 2015). The Fischer-Spier esterification pathway has multiple points where these free $H^+$ and $OH^-$ (from the plasma-based dissociation of water) groups provide the necessary catalyst for more interactions and a new pathway in the presence of these ions is proposed (Fig. 11). The free $H^+$ ions are considerably more reactive than the hydronium ions that typically initiate the esterification reaction (Munjal & Singh, 2020). Furthermore, the ions produced by the plasma were likely to be in a more energetic state (than static air), based on the high gas temperature and hence increased vibration and collision properties of the ions (Fig. 10a) (Li et al., 2018) which would have increased the favourability of the forward esterification reaction and hence the respective esters observed in Figs. 2, 3, 5, & 6.

Harris et al. (2020) found that an increase in cold plasma power increases methanol decomposition. They attributed this to an increase in electron energy and, hence, an increase in the bonds that can be cleaved. This suggests that the cold plasma may also have contributed to the increased reactivity of the methanol as well as the hexanoic and butanoic acids (Fig. 11). This may also explain why this was not seen in ethanol, as it has a longer chain and may be more protected from the cold plasma (Mulay & Rathod, 2022).

## 4. Conclusion

This research investigated the impact of cold plasma treatments of butanoic and hexanoic acid solutions in ethanol and methanol and their influence on their respective esterification. The type of gas affected the presence of butanoic acid and hexanoic acid (in the M1 solution of volatile compounds in methanol), with $N_2$ and Air-based plasmas significantly increasing the concentration compared to argon and none. When hexanoic acid was treated individually in methanol (HaM1), air-based plasma increased methyl hexanoate in both the liquid and headspace phases. This is evidence that cold plasma can potentially induce esterification and not just increase the volatility of esters. When butanoic acid and hexanoic acid were individually treated in ethanol, their headspace concentrations significantly increased. Despite this increase, unlike methanol, no observable esterification occurred in ethanol (either natural or induced). Real-time volatile headspace analysis (APCI-MS-MS-nose) corroborated these findings, demonstrating increased methyl esterification of butanoic acid and hexanoic acid. OES analysis revealed that air and argon-based plasmas contained reactive oxygen, hydrogen,

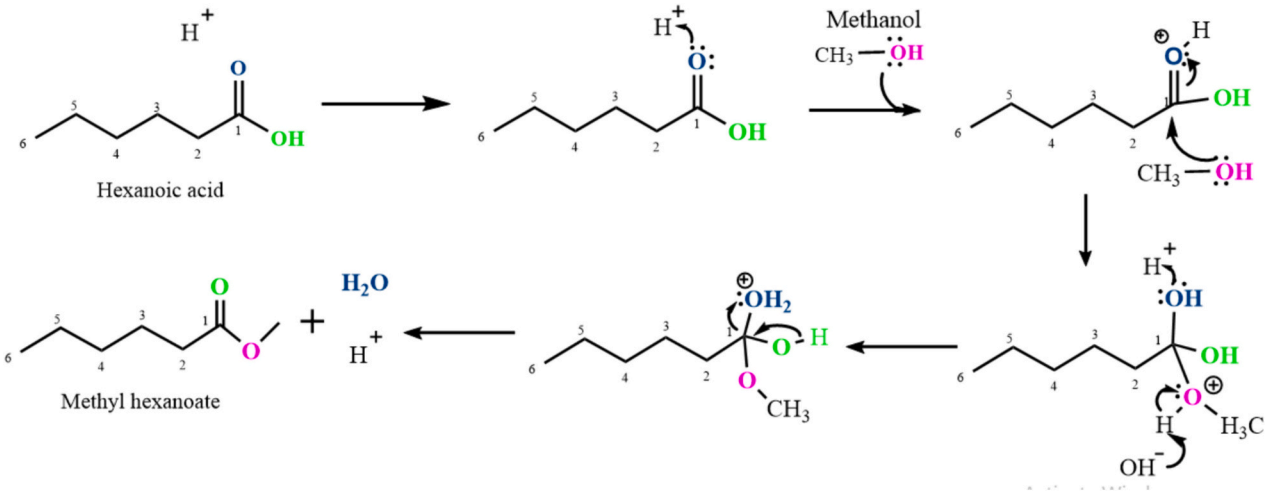


**Fig. 11.** Hypothesised Fischer-Spier esterification pathway of carboxylic acids and alcohols into esters, using hexanoic acid and methanol as an example (Hernández-Montelongo, García-Sandoval, & Aguilar-Garnica, 2015) with free $H^+$ and $OH^-$ ions emitted in the plasma as potential contributors to the pathway reactions. Compounds are colour-coded to show their transition within the pathway.

and nitrogen species: air-based plasma contained $N_2$, OH, $N_2^+$, $H_\alpha$, and O ions, whereas argon plasma contained substantially more O, $H_\gamma$, and OH ions, potentially explaining changes in esterification capability. This study proposed a new mechanism by which these ions influence and increase the formation of Fischer-Spier esters through interactions between the hydroxyl groups and free protons generated by the plasma's interaction with water in the air. OES analysis of the plasmas shows increased H and OH in the argon plasmas, increasing methyl hexanoate generation in the presence of other compounds. 3D cross-sectional OES analysis of argon-based plasma revealed a substantial decrease in the presence of all ions beyond ~10 mm in all directions from the plasma source. This study demonstrates that plasma could induce esterification, suggesting a cheaper and more efficient alternative to chemical catalysts like sulfuric acid. It also shows that argon-based RF plasma positioned <10 mm away from the sample may increase this process. Reducing this gap via liquid-based plasma devices could also increase this with a liquid-based Fourier transform infrared (FTIR) spectrometry analysis as a potential option for near real-time analysis of the plasma-ester interaction.

## CRediT authorship contribution statement

**George R. Warne:** Writing – original draft, Visualization, Methodology, Investigation, Formal analysis, Data curation. **Mui Lim:** Writing – review & editing. **Pradeep Lamichhane:** Writing – review & editing, Data curation. **Zdenko Machala:** Writing – review & editing. **Volker Hessel:** Writing – review & editing. **Philip M. Williams:** Writing – review & editing, Supervision, Funding acquisition. **Ian D. Fisk:** Writing – review & editing, Supervision, Funding acquisition, Conceptualization.

## Declaration of competing interest

The authors declare that there are no conflicts of interest in this paper.

## Data availability

Data will be made available on request.

## Acknowledgments

This work was supported by the Engineering and Physical Sciences Research Council [Grant number EP/R513283/1] awarded to the University of Nottingham, via a PhD studentship in Astropharmacy to GRW. The authors would also like to thank the Nottingham-Adelaide Alliance (the University of Nottingham and the University of Adelaide Joint Research Programme) for providing the resources required to conduct this study. The authors would also like to thank Kerry Wilkinson for their feedback on this paper.

## Appendix A. Supplementary data

Supplementary data to this article can be found online at https://doi.org/10.1016/j.ifset.2024.103726.

## References

Aanesland, A., Bredin, J., Chabert, P., & Godyak, V. (2012). Electron energy distribution function and plasma parameters across magnetic filters. *Applied Physics Letters, 100*(4), 1–4. https://doi.org/10.1063/1.3680088

Abdul-Majeed, W. S., Al-Thani, G. S., & Al-Sabahi, J. N. (2016). Application of flying jet plasma for production of biodiesel fuel from wasted vegetable oil. *Plasma Chemistry and Plasma Processing, 36*(1), 1517–1531. https://doi.org/10.1007/s11090-016-9735-0

Ahmad, N., Javed, F., Awan, J. A., Ali, S., Fazal, T., Hafeez, A., Aslam, R., Rashid, N., Rehman, M. S. U., Zimmerman, W. B., & Rehman, F. (2019). Biodiesel production intensification through microbubble mediated esterification. *Fuel, 253*(1), 25–31. https://doi.org/10.1016/j.fuel.2019.04.173

Akacha, N. B., & Gargouri, M. (2015). Microbial and enzymatic technologies used for the production of natural aroma compounds: Synthesis, recovery modelling, and bioprocesses. *Food and Bioproducts Processing, 94*(1), 675–706. https://doi.org/10.1016/j.fbp.2014.09.011

Asif, M., Javed, F., Younas, M., Gillani, M. A., Zimmerman, W. B., & Rehman, F. (2024). Investigating biodiesel production from chicken fat oil using bi-functional catalysts and microbubble mediated mass transfer. *Fuel, 358*(A), 130125–130134. https://doi.org/10.1016/j.fuel.2023.130125

Bao, Y., Reddivari, L., & Huang, J. Y. (2020). Development of cold plasma pre-treatment for improving phenolics extractability from tomato pomace. *Innovative Food Science & Emerging Technologies, 65*(102445), 1–9. https://doi.org/10.1016/j.ifset.2020.102445

Ben-Naim, A., & Marcus, Y. (1984). Solvation thermodynamics of nonionic solutes. *The Journal of Chemical Physics, 81*(4), 2016–2027. https://doi.org/10.1063/1.447824

Campelo, P. H., Alves Filho, E. G., Silva, L. M., de Brito, E. S., Rodrigues, S., & Fernandes, F. A. (2020a). Modulation of aroma and flavor using glow discharge plasma technology. *Innovative Food Science & Emerging Technologies, 62*(102363), 1–11. https://doi.org/10.1016/j.ifset.2020.102363

Campelo, P. H., Alves Filho, E. G., Silva, L. M., de Brito, E. S., Rodrigues, S., & Fernandes, F. A. (2020b). Modulation of aroma and flavor using dielectric barrier discharge plasma technology in a juice rich in terpenes and sesquiterpenes. *LWT-Food Science and Technology, 130*(109644), 1–9. https://doi.org/10.1016/j.lwt.2020.109644

Cubas, A. L. V., Machado, M. M., Pinto, C. R. S. C., Moecke, E. H. S., & Dutra, A. R. A. (2016). Biodiesel production using fatty acids from food industry waste using corona discharge plasma technology. *Waste Management, 47*(A), 149–154. https://doi.org/10.1016/j.wasman.2015.05.040

De Barros, D. P., Azevedo, A. M., Cabral, J. M., & Fonseca, L. P. (2012). Optimization of flavor esters synthesis by fusarium solani pisi cutinase. *Journal of Food Biochemistry, 36*(3), 275–284. https://doi.org/10.1111/j.1745-4514.2010.00535.x

Du, X., Plotto, A., Baldwin, E., & Rouseff, R. (2011). Evaluation of volatiles from two subtropical strawberry cultivars using GC–olfactometry, GC-MS odor activity values, and sensory analysis. *Journal of Agricultural and Food Chemistry, 59*(23), 12569–12577. https://doi.org/10.1021/jf2030924

Duignan, T. T., Parsons, D. F., & Ninham, B. W. (2015). Hydronium and hydroxide at the air–water interface with a continuum solvent model. *Chemical Physics Letters, 635*(1), 1–12. https://doi.org/10.1016/j.cplett.2015.06.002

Favell, J. W., Wilkinson, K. L., Zigg, I., Lyons, S. M., Ristic, R., Puglisi, C. J., … McKay, M. (2022). Correlating sensory assessment of smoke-tainted wines with inter-laboratory study consensus values for volatile phenols. *Molecules, 27*(15), 4892–4896. https://doi.org/10.3390/molecules27154892

Ghimire, B., Sornsakdanuphap, J., Hong, Y. J., Uhm, H. S., Weltmann, K. D., & Choi, E. H. (2017). The effect of the gap distance between an atmospheric-pressure plasma jet nozzle and liquid surface on OH and $N_2$ species concentrations. *Physics of Plasmas, 24*(7), 3502–3513. https://doi.org/10.1063/1.4989735

Golda, J., Biskup, B., Layes, V., Winzer, T., & Benedikt, J. (2020). Vacuum ultraviolet spectroscopy of cold atmospheric pressure plasma jets. *Plasma Processes and Polymers, 17*(6), 1900216–1900227. https://doi.org/10.1002/ppap.201900216

Harris, J., Zhang, K., & Phan, A. N. (2020). Cold plasma assisted decomposition of alcohols. *Chemical Engineering and Processing Process Intensification, 153*(107985), 1–11. https://doi.org/10.1016/j.cep.2020.107985

Hernández-Montelongo, R., García-Sandoval, J. P., & Aguilar-Garnica, E. (2015). On the non-ideal behavior of the homogeneous esterification reaction: A kinetic model based on activity coefficients. *Reaction Kinetics, Mechanisms and Catalysis, 115*(2), 401–419. https://doi.org/10.1007/s11144-015-0848-x

Istkhar, T., Hafeez, A., Javed, F., Fazal, T., Ahmad, F., Hussain, A., … Rehman, F. (2023). Intensification of esterification reaction microbubble mediated reactive distillation. *Chemical Engineering and Processing Process Intensification, 191*(1), Article 109435. https://doi.org/10.1016/j.cep.2023.109435

Janus, E., Ossowicz, P., Klebeko, J., Nowak, A., Duchnik, W., Kucharski, Ł., & Klimowicz, A. (2020). Enhancement of ibuprofen solubility and skin permeation by conjugation with L-valine alkyl esters. *RSC Advances, 10*(13), 7570–7584. https://doi.org/10.1039/D0RA00100G

Javed, F., Zimmerman, W. B., Fazal, T., Hafeez, A., Mustafa, M., Rashid, N., & Rehman, F. (2023). Green synthesis of biodiesel from microalgae cultivated in industrial wastewater via microbubble-induced esterification using bio-MOF-based heterogeneous catalyst. *Chemical Engineering Research and Design, 189*(1), 707–720. https://doi.org/10.1016/j.cep.2023.109435

Khan, Z., Javed, F., Shamair, Z., Hafeez, A., Fazal, T., Aslam, A., Zimmerman, W. B., & Rehman, F. (2021). Current developments in esterification reaction: A review on process and parameters. *Journal of Industrial and Engineering Chemistry, 103*(1), 80–101. https://doi.org/10.1016/j.jiec.2021.07.018

Klämpfl, T. G., Isbary, G., Shimizu, T., Li, Y. F., Zimmermann, J. L., Stolz, W., … Schmidt, H. U. (2012). Cold atmospheric air plasma sterilization against spores and other microorganisms of clinical interest. *Applied and Environmental Microbiology, 78*(15), 5077–5082. https://doi.org/10.1128/AEM.00583-12

Lester, S., Cornacchia, L., Corbier, C., Taylor, M. A., Ayed, C., Yang, N., … Fisk, I. (2021). Identification of aroma compounds in a commonly prescribed oral nutritional supplement and associated changes in olfactory abilities with human ageing. *Scientific Reports, 11*(1), 1–13. https://doi.org/10.1038/s41598-021-95915-6

Lester, S., Hurst, K., Cornacchia, L., Kleijn, M., Ayed, C., Dinu, V., … Fisk, I. (2021). The relation between stimulated salivary flow and the temporal consumption experience of a liquid oral nutritional supplement. *Appetite, 166*(105325), 1–14. https://doi.org/10.1016/j.appet.2021.105325

Li, H. P., Ostrikov, K. K., & Sun, W. (2018). The energy tree: Non-equilibrium energy transfer in collision-dominated plasmas. *Physics Reports, 770*(1), 1–45. https://doi.org/10.1016/j.physrep.2018.08.002

Li, M., Hu, Y., Lv, L., Fang, T., Hao, L., Li, S., Wu, Y., Dong, X., & Liu, H. (2023). Implementation of solvation free energy framework to predict the vapor-liquid equilibrium behaviors for the water–hydrazine and ethanol–water azeotropic systems. *Chemical Engineering Science, 275*(118751), 1–10. https://doi.org/10.1016/j.ces.2023.118751

Liu, Q., Wu, H., Luo, J., Liu, J., Zhao, S., Hu, Q., & Ding, C. (2021). Effect of dielectric barrier discharge cold plasma treatments on flavor fingerprints of brown rice. *Food Chemistry, 352*(129402), 1–9. https://doi.org/10.1016/j.foodchem.2021.129402

Lotfy, K. (2020). The impact of the carrier gas composition of non-thermal atmospheric pressure plasma jet for bacteria sterilization. *AIP Advances, 10*(1), 1–8. https://doi.org/10.1063/1.5099923

Machala, Z., Janda, M., Hensel, K., Jedlovský, I., Leštinská, L., Foltin, V., … Morvova, M. (2007). Emission spectroscopy of atmospheric pressure plasmas for bio-medical and environmental applications. *Journal of Molecular Spectroscopy, 243*(2), 194–201. https://doi.org/10.1016/j.jms.2007.03.001

Misra, N. N., Pankaj, S. K., Segat, A., & Ishikawa, K. (2016). Cold plasma interactions with enzymes in foods and model systems. *Trends in Food Science and Technology, 55*(1), 39–47. https://doi.org/10.1016/j.tifs.2016.07.001

Mulay, A., & Rathod, V. K. (2022). Kinetics, mass transfer, and thermodynamics of ethyl Hexanoate synthesis using heterogeneous catalyst. *Chemical Data Collections, 41*(100916), 1–12. https://doi.org/10.1016/j.cdc.2022.100916

Munjal, S., & Singh, A. (2020). *The Arrhenius acid and base theory. In Corrosion.* IntechOpen. https://doi.org/10.5772/intechopen.88173

Nagata, Y., Usui, K., & Bonn, M. (2015). Molecular mechanism of water evaporation. *Physical Review Letters, 115*(23), 1–5. https://doi.org/10.1103/PhysRevLett.115.236102

Pan, Y., Cheng, J. H., & Sun, D. W. (2019). Cold plasma-mediated treatments for shelf life extension of fresh produce: A review of recent research developments. *Comprehensive Reviews in Food Science and Food Safety, 18*(5), 1312–1326. https://doi.org/10.1111/1541-4337.12474

Pandiyaraj, K. N., Vasu, D., Padmanabhan, P. V. A., Pichumani, M., Deshmukh, R. R., & Kandavelu, V. (2020). Evaluation of influence of cold atmospheric pressure argon plasma operating parameters on degradation of aqueous solution of reactive blue 198 (RB-198). *Plasma Science and Technology, 22*(5), 5504–5516. https://doi.org/10.1088/2058-6272/ab568d

Pho, Q. H., Lin, L., Rebrov, E. V., Sarafraz, M. M., Tran, T. T., Tran, N. N., Losic, D., & Hessel, V. (2023). Process intensification for gram-scale synthesis of N-doped carbon quantum dots immersing a microplasma jet in a gas-liquid reactor. *Chemical Engineering Journal, 452*(1), 139164–139176. https://doi.org/10.1016/j.cej.2022.139164

Prat, L., Espinoza, M. I., Agosin, E., & Silva, H. (2014). Identification of volatile compounds associated with the aroma of white strawberries (*Fragaria chiloensis*). *Journal of the Science of Food and Agriculture, 94*(4), 752–759. https://doi.org/10.1002/jsfa.6412

Reuter, S., Von Woedtke, T., & Weltmann, K. D. (2018). The kINPen—A review on physics and chemistry of the atmospheric pressure plasma jet and its applications. *Journal of Physics D: Applied Physics, 51*(23), 233001–233052. https://doi.org/10.1088/1361-6463/aab3ad

Roy, N. C., Talukder, M. R., & Chowdhury, A. N. (2017). OH and O radicals production in atmospheric pressure air/Ar/H2O gliding arc discharge plasma jet. *Plasma Science and Technology, 19*(12), 125402–125411. https://doi.org/10.1088/2058-6272/aa86a7

Sarma, G. V. S., Kumar, G. S., Vijay, M., & Ramesh, K. V. (2021). Kinetic studies of esterification of butanoic acid with cyclohexanol. *Materials Today Proceedings, 46*(1), 737–739. https://doi.org/10.1016/j.matpr.2020.12.373

Silveira, M. R., Coutinho, N. M., Esmerino, E. A., Moraes, J., Fernandes, L. M., Pimentel, T. C., Freitas, M. Q., Silva, M. C., Raices, R. S., Ranadheera, C. S., & Borges, F. O. (2019). Guava-flavored whey beverage processed by cold plasma technology: Bioactive compounds, fatty acid profile and volatile compounds. *Food Chemistry, 279*(1), 120–127. https://doi.org/10.1016/j.foodchem.2018.11.128

Thirumdas, R., Sarangapani, C., & Annapure, U. S. (2014). Cold plasma: A novel non-thermal technology for food processing. *Food Biophysics, 10*(1), 1–11. https://doi.org/10.1007/s11483-014- 9382-z

Tomeková, J., Kyzek, S., Medvecká, V., Gálová, E., & Zahoranová, A. (2020). Influence of cold atmospheric pressure plasma on pea seeds: DNA damage of seedlings and optical diagnostics of plasma. *Plasma Chemistry and Plasma Processing, 40*(6), 1571–1584. https://doi.org/10.1007/s11090-020-10109-8

Warne, G. R., Lim, M., Wilkinson, K., Hessel, V., Williams, P. M., Coad, B., & Fisk, I. D. (2023). Radiofrequency cold plasma–a novel tool for flavour modification in fresh and freeze-dried strawberries. *Innovative Food Science & Emerging Technologies, 90*(103497), 1–15. https://doi.org/10.1016/j.ifset.2023.103497

Warne, G. R., Williams, P. M., Pho, H. Q., Tran, N. N., Hessel, V., & Fisk, I. D. (2021). Impact of cold plasma on the biomolecules and organoleptic properties of foods: A review. *Journal of Food Science, 86*(9), 3762–3777. https://doi.org/10.1111/1750-3841.15856

Xu, Y., Minhazul, K. A., & Li, X. (2020). The occurrence, enzymatic production, and application of ethyl butanoate, an important flavour constituent. *Flavour and Fragrance Journal, 35*(6), 601–615. https://doi.org/10.1002/ffj.3613

Zare, M., Golmakani, M. T., & Sardarian, A. (2020). Green synthesis of banana flavor using different catalysts: A comparative study of different methods. *Green Chemistry Letters and Reviews, 13*(2), 83–92. https://doi.org/10.1080/17518253.2020.1737739

Zhong, Y., Warren, G. L., & Patel, S. (2008). Thermodynamic and structural properties of methanol–water solutions using nonadditive interaction models. *Journal of Computational Chemistry, 29*(7), 1142–1152. https://doi.org/10.1002/jcc.20877

Zimmerman, W. B., & Kokoo, R. (2018). Esterification for biodiesel production with a phantom catalyst: Bubble mediated reactive distillation. *Applied Energy, 221*(1), 28–40. https://doi.org/10.1016/j.apenergy.2018.03.147